Acta Crystallographica Section D
Biological Crystallography
ISSN 0907-4449

Crystal packing of the c_6-type cytochrome OmcF from *Geobacter sulfurreducens* is mediated by an N-terminal Strep-tag II

Peer Lukat, Maren Hoffmann and Oliver Einsle*

Institut für Mikrobiologie und Genetik, Georg-August-Universität Göttingen, Justus-von-Liebig-Weg 11, 37077 Göttingen, Germany

Correspondence e-mail: oeinsle@uni-goettingen.de

Received 28 May 2008
Accepted 9 July 2008

PDB Reference: OmcF, 3dp5, r3dp5sf.

The putative outer membrane *c*-type cytochrome OmcF from *Geobacter sulfurreducens* contains a single haem group and shows homology to soluble cytochromes c_6, a class of electron-transfer proteins that are typically found in cyanobacterial photosynthetic electron-transfer chains. OmcF was over-expressed heterologously in *Escherichia coli* as an N-terminal Strep-tag II fusion protein and isolated using streptactin-affinity chromatography followed by size-exclusion chromatography. The structure was solved by Fe SAD using data collected to a resolution of 1.86 Å on a rotating copper-anode X-ray generator. In the crystal, packing interactions in one dimension were exclusively mediated through the Strep-tag II sequence. The tag and linker regions were in contact with three further monomers of OmcF, leading to a well defined electron-density map for this engineered and secondary-structure-free region of the molecule.

1. Introduction

Molecular dioxygen is the most efficient terminal electron acceptor available for a respiratory energy metabolism that couples electron transport along a redox-potential gradient to the translocation of protons across a biological membrane. In anoxic environments, the best electron acceptor is nitrate, NO_3^-, followed by metal ions such as Fe^{3+} or Mn^{4+} (Lovley, 1991, 1993, 1997). While gaseous dioxygen and soluble nitrate can be easily taken up by organisms, the oxides of iron and manganese are present in the form of insoluble minerals and hence are hard to access (Lovley *et al.*, 2004). Nevertheless, despite the obvious difficulties involved in respiring a solid substrate, bacteria have evolved three distinct strategies to achieve the reduction of metal oxides (Newman, 2001; DiChristina, 2005; DiChristina *et al.*, 2005). The most straightforward approach is to charge electrons onto small redox-active compounds that are subsequently expelled from the cell. Quinones and humic acids are used for this purpose and some of these carriers have been found to perform a double function as redox-active antibiotics (Newman & Kolter, 2000; Hernandez & Newman, 2001). The second possible strategy reverses the principle and makes use of siderophores. These again are small carrier molecules, but now acting as strong chelators for metal ions and being used to leech metals out of minerals that are subsequently reimported into the cell and reduced by periplasmic enzymes (Varma & Chincholkar, 2007; Chiu *et al.*, 2001). Both of these methods are by design limited in their control of electron and substrate flow and are therefore less efficient than the third mechanism,

© 2008 International Union of Crystallography
Printed in Singapore – all rights reserved

for which the term 'dissimilatory metal reduction' (DMR) was coined (Lovley, 1993). In DMR, electron-transfer systems cross both membranes of the Gram-negative metal-reducing bacteria and shuttle electrons to the outside of the cell, where they can be used to reduce the minerals *in situ*. This requires distinct transfer chains that terminate in metal reductases that are located on the outside of the bacterial cell.

The considerable interest in bacterial metal reduction originates not only from the geologically relevant role of DMR organisms in shaping the global environment during the entire history of life on Earth, but in particular from their wide range of possible biotechnological applications. Owing to the low substrate-specificity of metal-reducing bacteria, other potentially hazardous metals can be reduced, including chromium, cadmium and uranium, opening a range of possible applications in bioremediatory processes, with encouraging initial results having been reported (Lovley, 1995, 2001; Lovley & Coates, 1997). Furthermore, DMR bacteria have been shown to adhere to graphite electrodes and transfer electrons, opening up various technological possibilities from biosensors to 'soil batteries' that power electronic hardware in the field (Bond *et al.*, 2002; Bond & Lovley, 2003, 2005). In anoxic environments, DMR bacteria were found to dominate bacterial populations under conditions favouring respiration of mineral oxides (Coates *et al.*, 1996; Lovley *et al.*, 2004). The genera *Geobacter* and *Shewanella* were the first to be identified as true metal reducers and when their genome sequences became available a striking abundance of genes encoding *c*-type cytochromes became obvious (Heidelberg *et al.*, 2002; Methé *et al.*, 2003). The genome of the δ-proteobacterium *G. sulfurreducens* PCA, the paradigmatic model organism for DMR, has been annotated with no less than 111 genes for this class of proteins in which one or multiple haem groups are covalently linked to a protein chain *via* binding motifs of the general pattern C-X_n-C-H ($2 \leq n \leq 5$; Methé *et al.*, 2003). Several of these proteins have been studied as model systems for understanding the packing and interaction of haem groups in larger and more complex cytochromes (Heitmann & Einsle, 2005).

A total of 31 of the *c*-type cytochromes of *G. sulfurreducens* were predicted to be localized in the outer membrane (Methé *et al.*, 2003). Of these, the 104-amino-acid OmcF is among the smallest and it has been shown that its deletion has a significant effect on the ability of the bacteria to grow by reduction of iron(III) citrate and also on the expression of several other cytochromes, including the putative metal reductases OmcB, OmcC and OmcS (Kim *et al.*, 2005). Based on its sequence, OmcF (GSU2432; the naming scheme of the genome is according to http://www.tigr.org) was grouped with the family of cytochromes c_6; its closest relatives were found in other Geobacteraceae. Outside this genus, OmcF shows similarities to cyanobacterial cytochromes c_6 (28.9% sequence identity to *Synechocystis* sp. PCC6803 cytochrome c_6) and also to plant-type cytochromes c_{6A} (16.6% sequence identity to the protein from *Arabidopsis thaliana*). In cyanobacteria, cytochromes c_6 are found as electron carriers to cytochrome *c* oxidase and in both cyanobacteria and algae they transfer electrons from the cytochrome b_6f complex to photosystem I. In a subsequent publication, the localization of OmcF at the outer membrane was revised and an inner membrane location was proposed instead (Ding *et al.*, 2006). Using a search algorithm for lipoproteins, a putative lipidation site was indeed predicted at amino acid Cys19 of the OmcF sequence (Juncker *et al.*, 2003).

Here, we report the crystal structure of OmcF refined to a resolution of 1.86 Å. The protein was recombinantly expressed in *Escherichia coli* as a soluble Strep-tag II fusion protein. The structure was solved by single-wavelength anomalous dispersion of iron (Fe SAD) using data collected to high redundancy on a copper rotating-anode generator. OmcF shows the typical characteristics of a c_6-type cytochrome, but surprisingly its crystallization was found to be strictly dependent on the affinity tag, which participates actively in crystal contact formation.

2. Materials and methods

2.1. Expression and purification of recombinant OmcF

The gene encoding *omcF* was amplified by the polymerase chain reaction from genomic DNA of *G. sulfurreducens* PCA using the forward primer 5′-AAA**GAATTC**CGGAGGCG-GCGAGCTGTTCG-3′, which introduced an *Eco*RI restriction site (bold) and removed the first 75 nucleotides that comprise both the leader sequence predicted by *SignalP* (Bendtsen *et al.*, 2004) and the lipid-attachment site as predicted by *LIPOP* (Juncker *et al.*, 2003). The reverse primer, 5′-AAA**CTCGAG**TCATGGGAAGCTCGCCAC-3′, introduced an *Xho*I restriction site (bold) after the stop codon. The fragment was then cloned into a modified pET22b(+) expression vector (Merck-Novagen, Darmstadt, Germany) that provided an *ompA* leader sequence and an N-terminal Strep-tag II. The protein was expressed in *E. coli* BL21 (DE3) containing the accessory plasmid pEC86 that encodes the eight *ccm* genes required for the maturation of *c*-type cytochromes (Thöny-Meyer *et al.*, 1995). Freshly transformed bacteria were used to inoculate 5 ml overnight cultures which were incubated at 310 K. Expression cultures were grown without induction aerobically in 2 l Erlenmeyer flasks filled with 1 l LB medium in an incubator at 298 K and 220 rev min^{-1} for 20 h. Cell pellets were resuspended in 2 ml binding buffer (20 m*M* Tris–HCl buffer pH 8.0) per gram of cells (wet weight) and disrupted by five passages though a microfluidizer (Microfluidics, Newton, Massachusetts, USA) at a pressure of 0.55 MPa. Debris and membranes were removed by centrifugation at 100 000*g* for 1 h. The supernatant was applied onto a StrepTactin column (IBA, Göttingen, Germany; Schmidt & Skerra, 2007) with a bed volume of 16 ml using the ÄKTA Prime system (GE Healthcare, Freiburg, Germany). The column was developed with a step of 2.5 m*M* desthiobiotin in binding buffer and the eluted peak fraction was further concentrated using Vivaspin centrifugal concentration devices (Vivascience/Sartorius, Göttingen, Germany) with a cutoff of 5 kDa. The concentrated sample was subsequently applied to size-exclusion

Table 1
Data-collection and refinement statistics.

Values in parentheses are for the highest resolution shell.

Data-collection statistics	
X-ray wavelength (Å)	1.5418
Resolution limits (Å)	30–1.86 (1.96–1.86)
Space group	$P2_12_12$
Unit-cell parameters (Å)	a = 53.48, b = 40.13, c = 42.09
No. of observations	321255
No. of unique reflections	14750
Multiplicity	21.78
Completeness (%)	99.7 (98.5)
R_{merge}†	0.105 (0.4952)
$R_{p.i.m.}$‡	0.022 (0.1202)
$I/\sigma(I)$	23.50 (6.06)
Refinement statistics	
R_{cryst}	0.172
R_{free}§	0.216
R.m.s.d. in bond lengths (Å)	0.018
R.m.s.d. in bond angles (°)	1.79
Cruickshank's DPI¶ (Å)	0.15
Average B factor (Å^2)	22.1
No. of protein atoms	777
No. of water molecules	124
Ramachandran statistics, residues in (%)	
Most favoured regions	88
Allowed regions	12
Generously allowed regions	0
Disallowed regions	0

† $R_{merge} = \sum_{hkl}\sum_i |I_i(hkl) - \langle I(hkl)\rangle| / \sum_{hkl}\sum_i I_i(hkl)$. ‡ $R_{p.i.m.}$ was calculated according to Weiss & Hilgenfeld (1997). § For the calculation of R_{free}, 5% of reflections were chosen at random to constitute a test set. ¶ The diffraction precision index (DPI) was calculated according to Cruickshank (1999).

chromatography (Superdex S75 16/60, GE Healthcare, Freiburg, Germany) with 150 m*M* NaCl in 20 m*M* Tris–HCl buffer pH 8.0. The concentration of the purified protein was determined by the bicinchoninic acid method (Smith *et al.*, 1985) and the samples were analyzed by SDS–PAGE (Laemmli, 1970) and haem staining (Goodhew *et al.*, 1986).

2.2. Spectroscopy and redox titrations

Electron-excitation spectra were recorded on an Ultrospec 2100 Pro spectrophotometer (GE Healthcare, Freiburg, Germany) for various protein concentrations and for samples fully reduced by the addition of 25 m*M* sodium dithionite or fully oxidized with 10 m*M* $K_3[Fe(CN)_6]$. Molar extinction coefficients were calculated based on the absorption values of different samples at isosbestic points. Potentiometric redox titrations were carried out according to a modification of the protocol of Dutton (1978). 2 ml 24 µ*M* OmcF in 150 m*M* NaCl and 20 m*M* Tris–HCl buffer pH 8.0 and a mixture of five redox mediators (methyl viologen, juglone, 1,4-naphthoquinone, phenazine methosulfate and 1,2-naphthoquinone), each at a concentration of 0.4 µ*M*, were used in an anoxic cuvette. Exclusion of dioxygen was assured by retaining a positive pressure of 10 kPa N_2 in the cuvette throughout the experiment. Reduction was achieved by stepwise addition of 25 m*M* $Na_2S_2O_4$ solution pH 8.0, while 10 m*M* $K_3[Fe(CN)_6]$ was used for reoxidation. Spectra were recorded using an OceanOptics S2000 fibre-optic CCD spectrometer. The fraction of reduced protein was calculated from the relative change in the absorption at 552 nm (α-band). The custom-made Ag/AgCl redox electrode (Sensortechnik Meinsberg, Germany) was calibrated with quinhydrone. All obtained redox potentials were corrected for the standard hydrogen electrode.

2.3. Crystallization and structure determination of OmcF

Purified protein was used for crystallization screening at a concentration of 10 mg ml^{-1} in sitting-drop vapour-diffusion experiments. Drops consisting of 1 µl protein solution and 1 µl reservoir solution were equilibrated against 300 µl reservoir solution. Within 3 d of incubation at 293 K, clusters of crystal needles and small plates appeared in conditions containing 1.4–1.8 *M* $(NH_4)_2SO_4$, 2%(*w*/*v*) PEG 400 and 100 m*M* HEPES–NaOH buffer at pH 7.0–7.5. Serial dilutions of crushed crystals from these conditions were used for microseeding into crystallization conditions with lowered ammonium sulfate concentrations. Drops consisting of 1 µl protein solution and 1 µl reservoir solution were incubated against 300 µl reservoir solution for 2 h and 0.2 µl of diluted (1:100) crystal slush was then added. The crystals obtained by microseeding still grew in clusters, but a few individual three-dimensional crystals could be isolated for X-ray diffraction experiments on a MicroMax 007 rotating copper-anode X-ray source (Rigaku, Tokyo, Japan) equipped with a MAR345dtb image-plate detector (MAR Research, Hamburg, Germany). Crystals were cryoprotected by transfer into 2.4 *M* lithium sulfate, 2% PEG 400 and 100 m*M* HEPES–NaOH pH 7.0 and cooled to 100 K in a nitrogen-gas stream for data collection. Diffraction data were integrated and scaled using the programs *DENZO* and *SCALEPACK* (Otwinowski & Minor, 1997). *SHELXD* was used to localize the haem Fe atom (Sheldrick, 2008) and initial phasing was carried out with

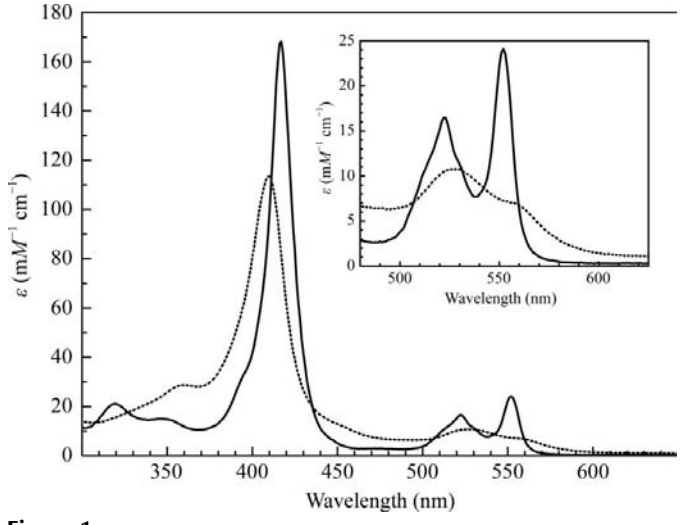

Figure 1
Electron-excitation spectra of recombinant *G. sulfurreducens* OmcF. Ferricyanide-oxidized (dotted line) and dithionite-reduced (unbroken line) spectra showed typical features of a *c*-type cytochrome, with a bathochromic shift of the Soret band upon reduction and an absorption maximum of the α-band in the reduced state at 552 nm. A shoulder above 610 nm in the oxidized spectrum indicative of high-spin Fe^{III} was not observed.

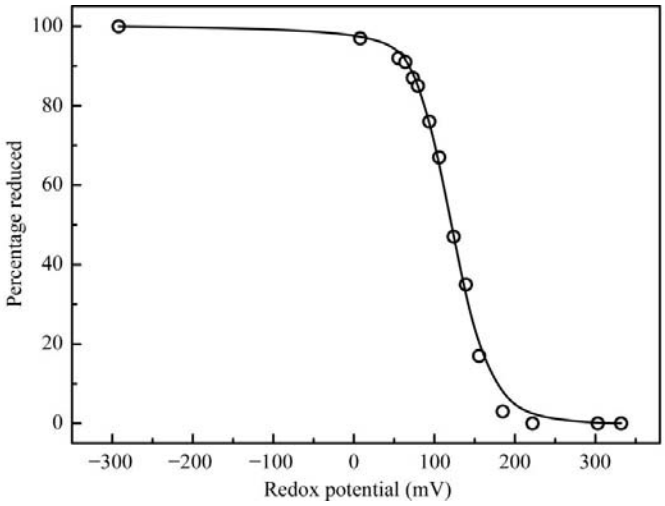

Figure 2
Potentiometric redox titration of *G. sulfurreducens* OmcF monitored at 552 nm. A nonlinear fit of the titration data with the Nernstian equation yields a midpoint potential of 121.2 ± 0.8 mV with respect to the standard hydrogen electrode.

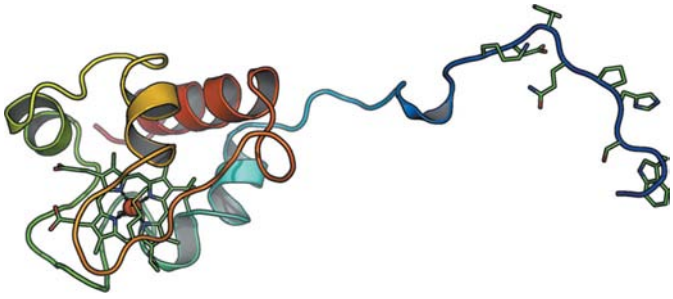

Figure 3
Crystal structure of *G. sulfurreducens* OmcF. The cartoon representation shows the elongated yet fully defined N-terminal region consisting of two amino acids originating from the cloning process (AS), the eight-amino-acid Strep-tag II (WSHPQFEK) and a nine-amino-acid linker region (GAETAVPNS). The cytochrome itself folds into the canonical globular fold of cytochromes c_6.

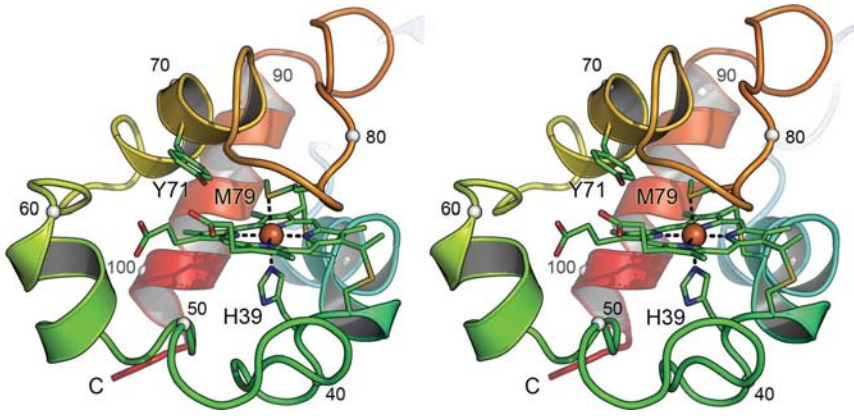

Figure 4
Stereo representation of the cytochrome c_6 domain of *G. sulfurreducens* OmcF. The single haem group of OmcF is covalently linked to the peptide chain *via* a bonding motif with sequence CAGCH (residues 35–39). His39 functions as a proximal axial ligand to the haem Fe atom, while the distal axial ligand is Met79. Every tenth residue in the sequence is marked.

SHELXE (Sheldrick, 2008). A single haem group was manually fitted into the electron-density map, allowing the identification of additional weak peaks in the anomalous difference electron-density map as the S atoms of cysteine and methionine. The positional information of these Fe and S atoms was used for phase calculations with *SHARP* (de La Fortelle *et al.*, 1997); *SOLOMON* (Abrahams & Leslie, 1996) was used for subsequent density modification. The structural model was built in *Coot* (Emsley & Cowtan, 2004) and refined using *REFMAC*5 (Murshudov *et al.*, 1997). Electrostatic potential maps were calculated using *DELPHI* (Honig & Nicholls, 1995) and figures were created in *PyMOL* (DeLano, 2002).

3. Results and discussion

3.1. Structure solution by Fe SAD

Data from a single diffracting crystal of OmcF were collected on a MAR345dtb image-plate detector using Cu $K\alpha$ radiation. The protein crystallized in the orthorhombic space group $P2_12_12$ with one monomer per asymmetric unit (Table 1). As amino-acid sequence comparisons with other cytochromes c_6 indicated strong homology, structure solution by molecular replacement was attempted as soon as the data completeness reached 70%. A moderately clear solution (CC = 0.24; R = 0.55) was obtained using *MOLREP* (Collaborative Computational Project, Number 4, 1994) with cytochrome c_{6A} from *A. thaliana* as a search model (PDB code 2ce0). However, the resulting crystal packing showed significant gaps in one dimension and the solution was consequently discarded and data collection was continued in order to obtain high-redundancy data for in-house phase determination by Fe SAD (Dauter *et al.*, 2002). At a multiplicity of 21 (Table 1), the haem Fe atom could be straightforwardly localized using *SHELXD* and a molecular model was built into an electron-density map obtained after phasing with *SHARP* and density modification with *SOLOMON* (see §2). The example of OmcF thus emphasizes the feasibility of using intrinsic Fe atoms for SAD phasing on in-house X-ray equipment. At λ = 1.54 Å the anomalous signal for iron is significantly stronger than that for sulfur (3.3 *versus* 0.6 electrons), such that Fe SAD phasing using diffraction data from a home source should be possible in most cases.

3.2. Biochemical and structural properties of OmcF

Oxidized and reduced electron-excitation spectra of OmcF show strong similarities to the spectra of previously characterized c_6 cytochromes (Fig. 1). The fully reduced spectrum exhibits three characteristic absorption maxima at 552 nm (α), 523 nm (β) and 417 nm (γ or Soret band). The molar extinction coefficient for the fully

Table 2
Comparison of structures of the cytochrome c_6 family.

PDB code	Organism	Type of organism	Resolution (Å)	R.m.s.d. (Å)	Sequence identity (%)	Reference
1gdv	*Porphyra yezoensis*	Red alga	1.56	0.88	25.2	Yamada *et al.* (2000)
2v08	*Phormidium laminosum*	Cyanobacterium	2.00	1.10	21.7	Worrall *et al.* (2007)
1f1f	*Arthrospira maxima*	Cyanobacterium	2.70	0.73	21.6	Sawaya *et al.* (2001)
1cyi	*Chlamydomonas rheinhardtii*	Green alga	1.90	0.91	21.5	Kerfeld *et al.* (1995)
1c6s	*Synechococcus elongatus*	Cyanobacterium	NMR	1.77	21.4	Beissinger *et al.* (1998)
1ctj	*Monoraphidium braunii*	Green alga	1.10	1.11	20.9	Frazão *et al.* (1995)
1ls9	*Cladophora glomerata*	Green alga	1.30	1.16	20.0	Dikiy *et al.* (2002)
1c6r	*Scenedesmus obliquus*	Green alga	1.90	1.07	18.3	Schnackenberg *et al.* (1999)
2ce0	*Arabidopsis thaliana*	Higher plant	1.24	1.84	16.6	Marcaida *et al.* (2006)

reduced α-band was determined as 23 800 M^{-1} cm^{-1}, which is in good agreement with previously reported values for cytochromes c_6 (Pettigrew & Moore, 1987; Moore & Pettigrew, 1990). The γ-band undergoes a hypsochromic shift to 410 nm in the oxidized spectrum. The absence of a shoulder around 610 nm points towards a low-spin configuration, as expected for a six-coordinate Fe^{III} in haem. The midpoint redox potential of OmcF was determined as 121.2 $\pm$ 0.8 mV by potentiometric redox titration (Fig. 2). This value is approximately 200 mV lower than those previously reported for cytochromes c_6 (Pettigrew & Moore, 1987; Moore & Pettigrew, 1990; Reuter & Wiegand, 2001), but well in accordance with the published midpoint potential of cytochrome c_{6A} from *A. thaliana* (Molina-Heredia *et al.*, 2003). At such low potential, the plant protein is unable to shuttle electrons between the cytochrome b_6f complex and photosystem I and consequently a regulatory role in photosynthesis or a function as a redox sensor was proposed (Weigel *et al.*, 2003). A sensory role has also been proposed for OmcF (Kim *et al.*, 2005), although dissimilatory iron reduction does not require as positive a potential as photosynthesis. Very recently, two novel c_6-type cytochromes from *Synechococcus* sp. PCC7002 were characterized and identified as members of two new groups of c_6-type cytochromes (Bialek *et al.*, 2008). One of these, PetJ2, exhibits a midpoint potential similar to cytochromes c_{6A}, with a sequence identity to OmcF of 22.4%.

In the electron-density map obtained for OmcF all residues of the protein were clearly defined (Figs. 3 and 4). The globular part of the structural model has a diameter of approximately 30 Å and comprises 79 amino acids, starting at residue 26 of the original OmcF sequence. In accordance with the classical fold of cytochromes c_6, it consists of four α-helical elements connected by three loop regions, one of which contains the CAGCH haem-binding motif which starts at Cys35 and immediately follows the first α-helix. The distal axial ligand of the haem iron, Met79, is located within the last loop region. This fold is highly similar to the known structures of cytochromes c_6 from unicellular algae and cyanobacteria (Kerfeld *et al.*, 1995; Beissinger *et al.*, 1998; Fig. 4). In addition to the canonical cytochrome fold, both the linker regions and

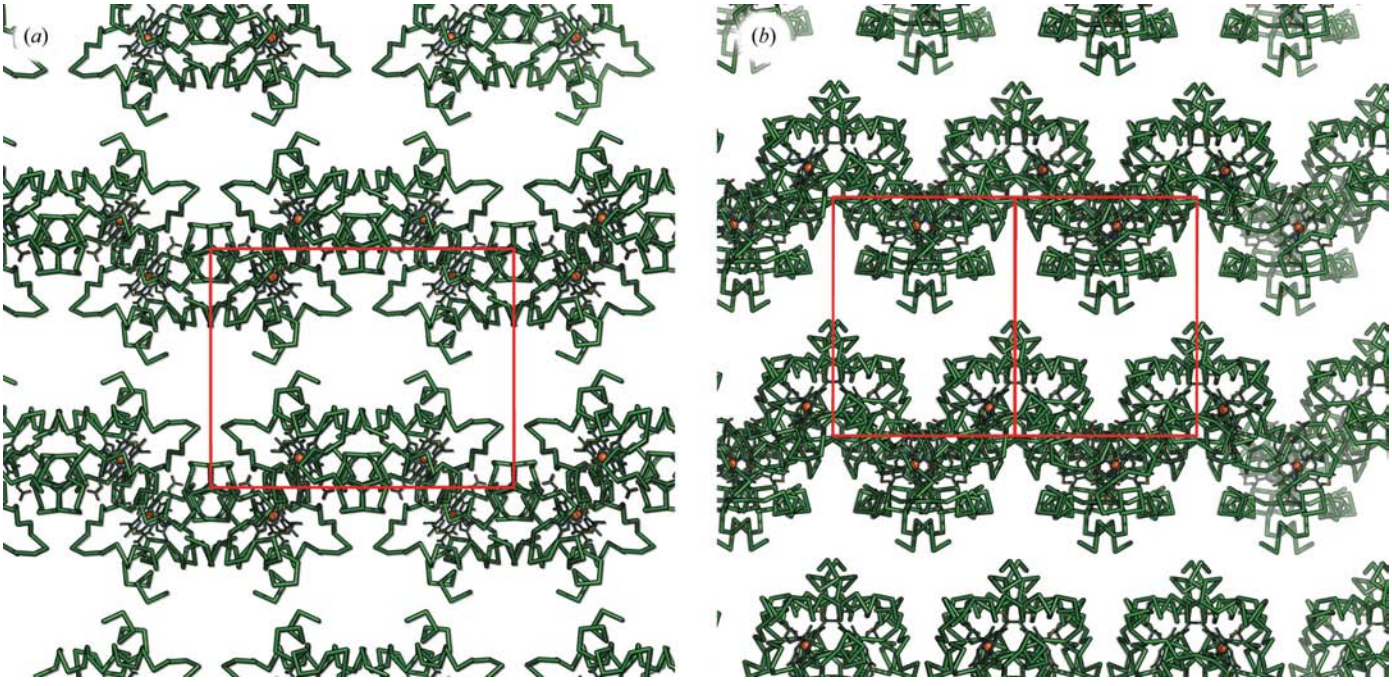

Figure 5
Packing interactions in crystals of *G. sulfurreducens* OmcF. The space group is $P2_12_12$, with the c axis pointing upward. The Strep-tag II affinity tag is omitted, emphasizing that it is required to provide packing along c. (*a*) shows a view along b, while (*b*) is rotated 45°, providing a view along the diagonal of the ab plane. One unit cell is shown in both figures.

Table 3
Listing of direct hydrogen bonds formed by the Strep-tag II/linker region.

The numbering of the tag and linker region is −15 to −1, with the Strep-tag II sequence encompassing residues −17 to −10. The original protein sequence of OmcF starts with residue Gly26, in accordance with the original gene sequence.

Strep-tag II/ linker position	Symmetry mate	Symmetry-mate position	Distance (Å)
His−15 $N^{\varepsilon 2}$	*A*	Tyr71 O^{η}	2.4; H_2O, 2.5
His−15 $N^{\varepsilon 2}$	*A*	Haem propionates	2.4; H_2O, 2.5/2.7
Glu−11 $O^{\varepsilon 1}$	*B*	Arg66 $N^{\eta 1}$	2.7
Glu−11 $O^{\varepsilon 2}$	*B*	Arg66 $N^{\eta 2}$	2.8
Lys−10 N	*C*	Ala101 O	2.9
Glu−7 O	*C*	Gln41 $N^{\varepsilon 2}$	2.9
Ala−5 O	*C*	Gln41 N	2.8

affinity tag (19 amino acids) that were part of the expressed construct of OmcF were clearly defined in electron density (Fig. 3; see below).

Close to the haem group a tyrosine residue, Tyr71, is oriented nearly parallel to the porphyrin plane, with its hydroxyl group coordinated to a water molecule bound between the haem propionates. Previously characterized cytochromes c_6 have a glutamine residue at the corresponding position, while in cytochromes c_{6A} a small hydrophobic residue (Val, Ile, Leu) was found (Chida *et al.*, 2006). Mutating this position in cytochromes c_6 and c_{6A} modulates the midpoint redox potential of the haem group (Worrall *et al.*, 2007). Tyr71 and its π-stacking with the porphyrin ring is the most significant difference between OmcF and cytochromes c_6, indicating that this feature may be a prime contributor to the significantly lower redox potential of OmcF. The family of cytochromes c_6 shows high structural conservation to the extent that all structures presented to date align with root-mean-squared deviations of their backbone positions of below 2 Å (Table 2). OmcF is the only protein in the list from a nonphotosynthetic organism and yet the protein shows higher homology to cytochromes c_6 than to other bacterial mono-haem cytochromes of known structure.

3.3. Crystallization of OmcF strictly depends on the affinity tag

The structural model of *G. sulfurreducens* OmcF quickly revealed that the solutions obtained by molecular replacement had actually been correct and that in the crystal packing, layers of protein were indeed separated by marked gaps (Fig. 5). These gaps were bridged exclusively by the N-terminal extension of the protein consisting of the Strep-tag II affinity tag used for protein purification and a nine-amino-acid linker sequence that was introduced during the cloning procedure. Crystallization of OmcF therefore necessarily depended on the presence of this linker and tag region. In crystal structures of engineered proteins affinity tags rarely have defined electron density, indicating structural flexibility. While presumably also flexible in solution, the Strep-tag II of OmcF was able to form favourable crystal contacts with a total of three monomers within the crystal packing, making it a crucial element in crystal formation in this case (Fig. 6). In this process, the strongly positive electrostatic surface potential of OmcF (not shown) may combine favourably with electron-rich amino-acid side chains in the affinity tag to allow stable packing interactions.

The number of direct hydrogen-bonding interactions between the Strep-tag II and its three interaction partners is limited to two each with the first and second molecules and three with the third (Table 3, Fig. 7). The first residues of the linker, Ala−5 to Ser−1, span the gap observed in the crystal packing (Fig. 5), reaching the next layer of protein where all interactions of the N-terminal segment take place. Intramolecular hydrogen bonds induce two structured conformations within this segment. One of these is a 3_{10}-helical turn from Gly−9 to Thr−6 and from this structure the two hydrogen bonds to Gln41 of the adjacent monomer are formed (Table 3, Fig. 7). A second structural unit comprises the region from Gln−13 to Lys−10 within the Strep-tag II. Here, the side chains of Gln−13, Glu−11 and Lys−10 form multiple hydrogen-bonding interactions to backbone amide groups, positioning the side chain of Glu−11 such that a tight salt bridge is formed with Arg66 from the second monomer in

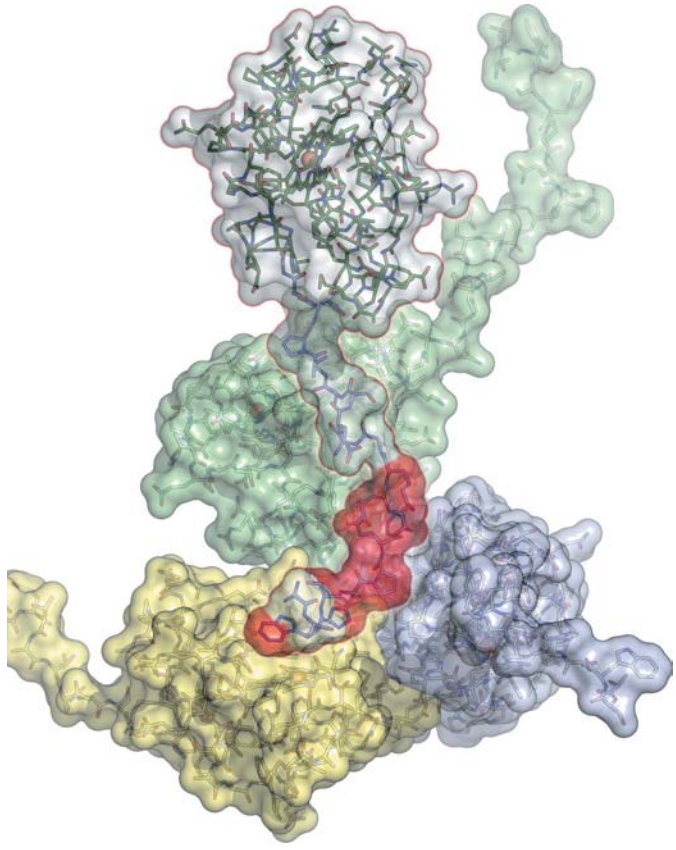

Figure 6
The Strep-tag II affinity tag mediates essential crystal contacts in *G. sulfurreducens* OmcF. The elongated N-terminal extension consisting of the affinity tag and a nine-amino-acid linker region bridges a gap in the crystal packing along the *c* axis (Fig. 5) to reach the next layer of proteins, where it makes specific contact with three OmcF monomers (green, blue and yellow). The residues of the Strep-tag II sequence (WSHPQFEK) are shown with a red surface.

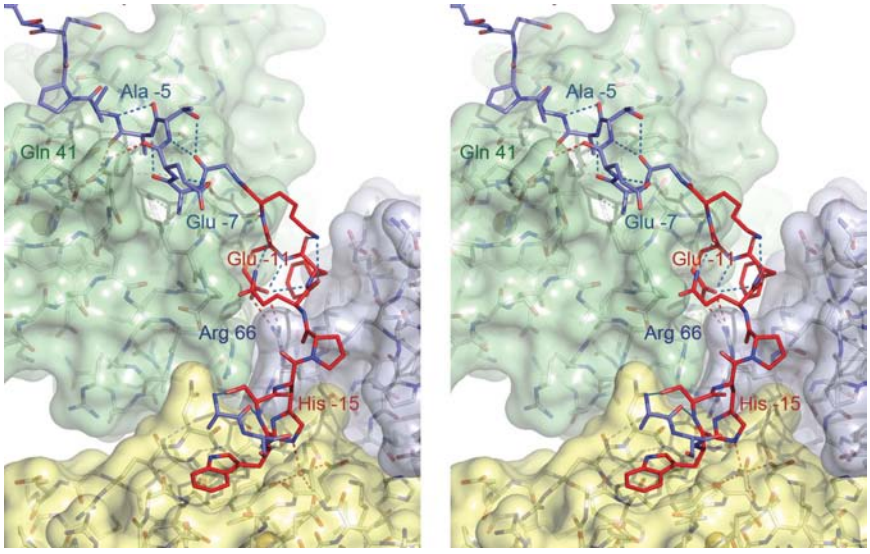

Figure 7
Stereo representation showing the interactions of the linker (blue) and Strep-tag II region (red) with three neighbouring monomers as detailed in Table 3. Hydrogen-bonding interactions within the linker/tag are shown in blue and interactions with other monomers in red. Five of the seven observed hydrogen-bonding interactions are formed by the Strep-tag II and the other two are formed by the linker region.

the crystal packing (Table 3, Fig. 7). The interaction with the third monomer crucially depends on a coordinated water molecule, the exact one described above to reside between the two propionate side chains of the haem group and Tyr71 (Fig. 7). In addition, the aromatic side chains of Phe−12 and Trp−17 and also Pro−3 and Pro−14 contribute to extensive van der Waals interactions that add favourably to the stability of the observed packing arrangement. Structured affinity tags are rarely observed in crystal structures and when they are they do not commonly participate in building up the crystal lattice, as they are not likely to form rigid structures. An exception was found in the structure of the yeast cytochrome bc_1 complex crystallized with a C-terminally Strep-tagged antibody Fv fragment (Hunte *et al.*, 2000). In this structure, crystal packing of the large membrane complex was mediated in one dimension by the bound Fv fragment, but half of a Strep-tag I sequence at the C-terminus of this fragment made a hydrogen-bonding interaction with a neighbouring bc_1 complex, contributing (although not exclusively) to the interaction between the molecules in the crystal.

This work was supported by Deutsche Forschungsgemeinschaft (grant Ei-520/1 and IRTG 1422). The plasmid pEC86 was a kind gift from Professor Linda Thöny-Meyer (EMPA, St Gallen, Switzerland).

References

Abrahams, J. P. & Leslie, A. G. W. (1996). *Acta Cryst.* D**52**, 30–42.
Beissinger, M., Sticht, H., Sutter, M., Ejchart, A., Haehnel, W. & Rosch, P. (1998). *EMBO J.* **17**, 27–36.
Bendtsen, J. D., Nielsen, H., von Heijne, G. & Brunak, S. (2004). *J. Mol. Biol.* **340**, 783–795.
Bialek, W., Nelson, M., Tamiola, K., Kallas, T. & Szczepaniak, A. (2008). *Biochemistry*, **47**, 5515–5522.
Bond, D. R., Holmes, D. E., Tender, L. M. & Lovley, D. R. (2002). *Science*, **295**, 483–485.
Bond, D. R. & Lovley, D. R. (2003). *Appl. Environ. Microbiol.* **69**, 1548–1555.
Bond, D. R. & Lovley, D. R. (2005). *Appl. Environ. Microbiol.* **71**, 2186–2189.
Chida, H., Yokoyama, T., Kawai, F., Nakazawa, A., Akazaki, H., Takayama, Y., Hirano, T., Suruga, K., Satoh, T., Yamada, S., Kawachi, R., Unzai, S., Nishio, T., Park, S. Y. & Oku, T. (2006). *FEBS Lett.* **580**, 3763–3768.
Chiu, H.-J., Johnson, E., Schröder, I. & Rees, D. C. (2001). *Structure*, **9**, 311–319.
Coates, J. D., Phillips, E. J. P., Lonergan, D. J., Jenter, H. & Lovley, D. R. (1996). *Appl. Environ. Microbiol.* **62**, 1531–1536.
Collaborative Computational Project, Number 4 (1994). *Acta Cryst.* D**50**, 760–763.
Cruickshank, D. W. J. (1999). *Acta Cryst.* D**55**, 583–601.
Dauter, Z., Dauter, M. & Dodson, E. J. (2002). *Acta Cryst.* D**58**, 494–506.
DeLano, W. L. (2002). *The PyMOL Molecular Graphics System.* Palo Alto, USA: DeLano Scientific.
DiChristina, T. J. (2005). *Geochim. Cosmochim. Acta*, **69**, A670.
DiChristina, T. J., Fredrickson, J. K. & Zachara, J. M. (2005). *Mol. Geomicrobiol.* **59**, 27–52.
Dikiy, A., Carpentier, W., Vandenberghe, I., Borsari, M., Safarov, N., Dikaya, E., Van Beeumen, J. & Ciurli, S. (2002). *Biochemistry*, **41**, 14689–14699.
Ding, Y. H., Hixson, K. K., Giometti, C. S., Stanley, A., Esteve-Nunez, A., Khare, T., Tollaksen, S. L., Zhu, W., Adkins, J. N., Lipton, M. S., Smith, R. D., Mester, T. & Lovley, D. R. (2006). *Biochim. Biophys. Acta*, **1764**, 1198–1206.
Dutton, P. L. (1978). *Methods Enzymol.* **54**, 411–435.
Emsley, P. & Cowtan, K. (2004). *Acta Cryst.* D**60**, 2126–2132.
Frazão, C., Soares, C. M., Carrondo, M. A., Pohl, E., Dauter, Z., Wilson, K. S., Hervas, M., Navarro, J. A., De la Rosa, M. A. & Sheldrick, G. M. (1995). *Structure*, **3**, 1159–1169.
Goodhew, C. F., Brown, K. R. & Pettigrew, G. W. (1986). *Biochim. Biophys. Acta*, **852**, 288–294.
Heidelberg, J. F. *et al.* (2002). *Nature Biotechnol.* **20**, 1118–1123.
Heitmann, D. & Einsle, O. (2005). *Biochemistry*, **44**, 12411–12419.
Hernandez, M. E. & Newman, D. K. (2001). *Cell. Mol. Life Sci.* **58**, 1562–1571.
Honig, B. & Nicholls, A. (1995). *Science*, **268**, 1144–1149.
Hunte, C., Koepke, J., Lange, C., Rossmanith, T. & Michel, H. (2000). *Structure*, **8**, 669–684.
Juncker, A. S., Willenbrock, H., Von Heijne, G., Brunak, S., Nielsen, H. & Krogh, A. (2003). *Protein Sci.* **12**, 1652–1662.
Kerfeld, C. A., Anwar, H. P., Interrante, R., Merchant, S. & Yeates, T. O. (1995). *J. Mol. Biol.* **250**, 627–647.
Kim, B. C., Leang, C., Ding, Y. H., Glaven, R. H., Coppi, M. V. & Lovley, D. R. (2005). *J. Bacteriol.* **187**, 4505–4513.
Laemmli, U. K. (1970). *Nature (London)*, **227**, 680–685.
La Fortelle, E. de, Irwin, J. J. & Bricogne, G. (1997). *Crystallographic Computing 7*, edited by P. E. Bourne & K. D. Watenpaugh, pp. 1–9. Oxford University Press.
Lovley, D. R. (1991). *Microbiol. Rev.* **55**, 259–287.
Lovley, D. R. (1993). *Annu. Rev. Microbiol.* **47**, 263–290.
Lovley, D. R. (1995). *J. Ind. Microbiol.* **14**, 85–93.
Lovley, D. R. (1997). *FEMS Microbiol. Rev.* **20**, 305–313.

Lovley, D. R. (2001). *Science*, **293**, 1444–1446.
Lovley, D. R. & Coates, J. D. (1997). *Curr. Opin. Biotechnol.* **8**, 285–289.
Lovley, D. R., Holmes, D. E. & Nevin, K. P. (2004). *Adv. Microb. Physiol.* **49**, 219–286.
Marcaida, M. J., Schlarb-Ridley, B. G., Worrall, J. A., Wastl, J., Evans, T. J., Bendall, D. S., Luisi, B. F. & Howe, C. J. (2006). *J. Mol. Biol.* **360**, 968–977.
Methé, B. A. *et al.* (2003). *Science*, **302**, 1967–1969.
Molina-Heredia, F. P., Wastl, J., Navarro, J. A., Bendall, D. S., Hervas, M., Howe, C. J. & De La Rosa, M. A. (2003). *Nature (London)*, **424**, 33–34.
Moore, G. R. & Pettigrew, G. W. (1990). *Cytochromes c: Evolutionary, Structural and Physicochemical Aspects.* Berlin: Springer.
Murshudov, G. N., Vagin, A. A. & Dodson, E. J. (1997). *Acta Cryst.* D**53**, 240–255.
Newman, D. K. (2001). *Science*, **292**, 1312–1313.
Newman, D. K. & Kolter, R. (2000). *Nature (London)*, **405**, 94–97.
Otwinowski, Z. & Minor, W. (1997). *Methods Enzymol.* **276**, 307–326.
Pettigrew, G. W. & Moore, G. R. (1987). *Cytochromes c: Biological Aspects.* Berlin: Springer.
Reuter, W. & Wiegand, G. (2001). In *Handbook of Metalloproteins*, edited by A. Messerschmidt, R. Huber, K. Wieghardt & T. Poulos. New York: John Wiley & Sons.
Sawaya, M. R., Krogmann, D. W., Serag, A., Ho, K. K., Yeates, T. O. & Kerfeld, C. A. (2001). *Biochemistry*, **40**, 9215–9225.
Schmidt, T. G. & Skerra, A. (2007). *Nature Protocols*, **2**, 1528–1535.
Schnackenberg, J., Than, M. E., Mann, K., Wiegand, G., Huber, R. & Reuter, W. (1999). *J. Mol. Biol.* **290**, 1019–1030.
Sheldrick, G. M. (2008). *Acta Cryst.* A**64**, 112–122.
Smith, P. K., Krohn, R. I., Hermanson, G. T., Mallia, A. K., Gartner, F. H., Provenzano, M. D., Fujimoto, E. K., Goeke, N. M., Olson, B. J. & Klenk, D. C. (1985). *Anal. Biochem.* **150**, 76–85.
Thöny-Meyer, L., Fischer, F., Kunzler, P., Ritz, D. & Hennecke, H. (1995). *J. Bacteriol.* **177**, 4321–4326.
Varma, A. & Chincholkar, S. B. (2007). Editors. *Microbial Siderophores.* New York: Springer.
Weigel, M., Varotto, C., Pesaresi, P., Finazzi, G., Rappaport, F., Salamini, F. & Leister, D. (2003). *J. Biol. Chem.* **278**, 31286–31289.
Weiss, M. S. & Hilgenfeld, R. (1997). *J. Appl. Cryst.* **30**, 203–205.
Worrall, J. A., Schlarb-Ridley, B. G., Reda, T., Marcaida, M. J., Moorlen, R. J., Wastl, J., Hirst, J., Bendall, D. S., Luisi, B. F. & Howe, C. J. (2007). *J. Am. Chem. Soc.* **129**, 9468–9475.
Yamada, S., Park, S.-Y., Shimizu, H., Koshizuka, Y., Kadokura, K., Satoh, T., Suruga, K., Ogawa, M., Isogai, Y., Nishio, T., Shiro, Y. & Oku, T. (2000). *Acta Cryst.* D**56**, 1577–1582.